

Fully Implicit Shock Tracking

J. B. BELL*, G. R. SHUBIN*, AND J. M. SOLOMON

*Naval Surface Weapons Center, White Oak Lab,
Silver Spring, Maryland 20910*

Received January 8, 1982

A fully implicit shock tracking method for solving hyperbolic free boundary problems arising in fluid dynamics is presented. The new method is based on the noniterative implicit methods developed by Beam and Warming and others. The principal feature of the new approach is that the implicit form is used to treat both interior points and boundary conditions simultaneously. In particular, the location of the free boundary (shock) surface is treated implicitly and coupled with all other unknowns. The method is presented here in the context of unsteady one-dimensional flow in a variable area duct with an internal shock wave. The fully implicit method and other strategies for advancing the shock are compared for computing a steady solution via a time asymptotic approach. Issues regarding extension of the method to multiple dimensions are also discussed.

1. INTRODUCTION

In this paper we develop a fully implicit shock tracking (or fitting) method for one-dimensional flow in a variable area duct. The method is based on the noniterative implicit methods described, for example, in Beam and Warming [1]. Implicit methods have recently become popular for fluid dynamics problems, especially when using a time asymptotic approach to obtain steady state solutions (see, e.g., [2-4]). The reason for this popularity is that implicit methods (based on von Neumann stability properties) allow a larger time step than is possible for explicit methods and consequently reduce the number of steps needed to reach a steady solution. In practical problems such as the supersonic blunt body problem, however, we can often improve the accuracy and efficiency of computations by tracking at least some of the shockwaves present in the problem. This entails using the tracked shock as a computational boundary, the geometry of which is unknown and is to be determined. Existing applications of implicit methods to such problems treat the shock geometry explicitly (e.g., [4]). It then becomes questionable whether the large time steps allowed at interior points can in fact be taken since the explicit advancement of the shock could impose restrictive bounds on step size.

The fully implicit method presented here (see Section 3) addresses this issue by treating both the interior flow equations and the boundary conditions in an implicit

* Current address: Exxon Production Research Co., P.O. Box 2189, Houston, Texas 77001.

fully coupled time-accurate manner. This approach is rather complicated and requires more work per step than is needed when treating boundaries explicitly. The allowable time step also increases, however, in some cases quite dramatically. For comparison purposes, we also consider a method which explicitly advances the shock. In addition, we develop an implicit but uncoupled approach which enjoys some of the advantages of the fully implicit method without the attendant increase in work per step (see Section 3).

Section 4 contains a detailed study of the computational efficiency of three methods for computing steady state solutions. It should be noted that to some extent the dramatic results for the fully implicit method are related to the one-dimensionality of the model problem. In the limit as time step size goes to infinity, the fully implicit method reduces to Newton's method [5], which provides an extremely efficient technique for computing steady solutions when a good initial guess is available [6]. Unfortunately, in multidimensional problems, the associated matrix problem becomes prohibitively large and operator splitting or approximate factorization is generally used. In this case the reduction to Newton's method will not occur and splitting error will limit the allowable size of time steps. Issues relating to the extension of implicit shock tracking methods to several dimensions will be discussed more fully in Section 5.

2. ANALYTIC FORMULATION

In this section we formulate a model problem on which to illustrate the fully implicit method. We wish to compute the steady one-dimensional flow in a duct of variable cross-sectional area $A(x)$ using a time asymptotic approach. The unsteady duct flow is described in physical space $0 \leq x \leq x_{\max}$ by

$$\frac{\partial(A\mathcal{U})}{\partial t} + \frac{\partial(A\mathcal{F})}{\partial x} - \mathcal{H} = 0, \quad (1)$$

where

$$\mathcal{U} = \begin{pmatrix} \rho \\ \rho u \\ \rho E \end{pmatrix}, \quad \mathcal{F} = \begin{pmatrix} \rho u \\ \rho u^2 + p \\ (\rho E + p)u \end{pmatrix}, \quad \mathcal{H} = \frac{dA}{dx} \begin{pmatrix} 0 \\ p \\ 0 \end{pmatrix},$$

and ρ is density, u is velocity, $E = e + \frac{1}{2}u^2$, where e is specific internal energy, and p is pressure. For simplicity the equation of state is chosen to be that of a perfect gas, $p = (\gamma - 1)\rho e$.

For certain duct shapes $A(x)$ and boundary specifications (discussed later), a steady solution exists in which a shock stands at some location in the duct. For numerical solution we shall not treat the problem in the form of (1) because of the difficulties associated with resolving the shock. Instead, we shall use a tracking

procedure in which the shock location is treated as a dependent variable. This is accomplished by transforming the problem to a computational space (ξ, τ) in which the physical shock location $s(t)$ is forced to be at a fixed location. An example of a transformation which does this is given by the mapping to computational space

$$\begin{aligned} \tau &= t, \\ \xi &= \xi(x, t) = x/s(t), & 0 \leq x \leq s(t), \\ &= 1 + (K - 1)[(x - s(t))/(x_{\max} - s(t))], & s(t) \leq x \leq x_{\max}, \end{aligned} \tag{2}$$

so that the physical shock location s is mapped into the internal computational boundary $\xi = 1$. Likewise the inflow location $x = 0$ and the outflow location $x = x_{\max}$ are mapped into $\xi = 0$ and $\xi = K$, respectively (see Fig. 1).

Under transformation (2) the governing equations in computational space (ξ, τ) can be written in the weak conservation form [7]

$$\partial U / \partial \tau = -(\partial F / \partial \xi) + (1/J)\mathcal{R} \equiv R_1(\xi; U, s, s_t), \tag{3}$$

where $U = A\mathcal{U}/J$, $F = \xi_t U + A\xi_x \mathcal{F}/J$ and $J = \xi_x$ is the Jacobian, for fixed τ , of transformation (2).

It remains to specify the boundary conditions at inflow ($\xi = 0$), outflow ($\xi = K$), and at the shock ($\xi = 1$). Appropriate boundary conditions can be determined by a characteristic analysis of the system. Such an analysis is presented in detail in Appendix A for the case of supersonic inflow and subsonic outflow with an internal shock with flow crossing the shock from left to right.

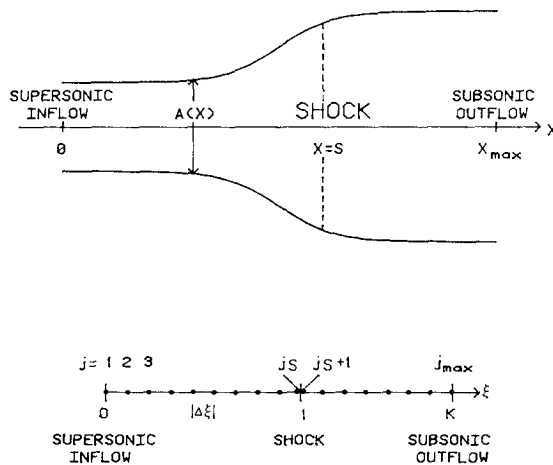


FIG. 1. Physical and computational spaces for duct problem.

At the supersonic inflow all flow quantities are specified so that

$$U(0, \tau) = sA(0) \begin{pmatrix} \rho_0 \\ \rho_0 u_0 \\ \rho_0(e_0 + u_0^2/2) \end{pmatrix}, \quad (4)$$

where the subscript "0" refers to the specified inflow quantities. At the subsonic outflow boundary ($\xi = K$), only the density ρ_e is specified; hence,

$$U_1(K, \tau) = A(x_{\max})(x_{\max} - s)/(K - 1) \rho_e. \quad (5a)$$

In addition, two compatibility conditions must be satisfied on $\xi = K$. These can be written in the form

$$\begin{aligned} \frac{\partial}{\partial \tau} \begin{pmatrix} U_2 \\ U_3 \end{pmatrix}_{\xi=K} &= \mathbf{TR}_1(K; U, s, s_t) + \frac{A(x_{\max})}{K-1} \left[\rho_e s_t - (x_{\max} - s) \frac{d\rho_e}{dt} \right] B \\ &\equiv R_2(U, s, s_t), \end{aligned} \quad (5b)$$

where

$$B = - \begin{pmatrix} u_e - a_e \\ (a_e^2/(\gamma - 1)) - u_e(a_e - \frac{1}{2}u_e) \end{pmatrix}, \quad \mathbf{T} = \begin{pmatrix} B & 1 & 0 \\ 0 & 1 & 1 \end{pmatrix},$$

with the "e" subscript denoting quantities at the outflow boundary and "a" the sound speed $(\gamma p/\rho)^{1/2}$.

The shock $\xi = 1$ represents an internal boundary. Quantities at the left (the low pressure side) will be denoted with an "L" subscript and quantities at the right (the high pressure side) will be denoted with an "R" subscript. The flow quantities on both sides of the shock must satisfy the Rankine-Hugoniot relations. These can be written in the form

$$U_R = \mathcal{R}(U_L, s, s_t). \quad (6)$$

The vector-valued function \mathcal{R} is given explicitly in Appendix B for a perfect gas with constant γ . On the left side of the shock, all of the original equations (3) hold with the ξ partial derivatives interpreted using only quantities on the left side (i.e., $0 < \xi \leq 1$). On the right side of the shock (the high pressure side), only one compatibility condition need be satisfied. This condition combined with the Rankine-Hugoniot relations differentiated with respect to τ gives the following equation for s_t :

$$\begin{aligned} \frac{\partial s_t}{\partial \tau} &= \alpha_1 \cdot \left[\frac{\partial(\xi_x U/A)}{\partial \xi} \right]_R - \alpha_2 \cdot \left[\frac{\partial(\xi_x U/A)}{\partial \xi} \right]_L + \alpha_3 \left(\frac{1}{A} \frac{dA}{dX} \right)_{\xi=1} \\ &\equiv r_3(U, s, s_t), \end{aligned}$$

where α_1 , α_2 , and α_3 are defined in Appendix A. Thus, the equations for s and s_t can be summarized in the form

$$\frac{\partial S}{\partial \tau} = \begin{pmatrix} s_t \\ r_3(U, s, s_t) \end{pmatrix} \equiv R_3(U, s, s_t), \quad S = \begin{pmatrix} s \\ s_t \end{pmatrix}. \quad (7)$$

The transformed form of Eq. (3) and boundary conditions (4)–(7) fully specify the problem to be discretized.

3. NUMERICAL METHODS

The implicit methods considered here are based on generalized time differencing in delta form introduced by Warming and Beam [8]. Namely, for any vector of unknowns W satisfying a system of equations of the form

$$\partial W / \partial \tau = R(\xi, \tau; W),$$

we have

$$\begin{aligned} \Delta W^n - c_1 h \Delta(R(\xi, \tau^n; W^n)) &= c_2 \Delta W^{n-1} + c_3 h R(\xi, \tau^n; W^n) \\ &+ [2c_1 - (1 + \pi^2 c_2)] O(h^2) + O(h^3), \end{aligned} \quad (8)$$

where $\Delta(\cdot)^n = (\cdot)^{n+1} - (\cdot)^n$, $h = \tau^{n+1} - \tau^n$, $\pi = (\tau^n - \tau^{n-1})/h$, $c_3 = 1 - \pi c_2$, and c_1 and c_2 are scalar parameters.

Fully Implicit Shock Tracking (FIST)

The FIST approach is to consider both the conservation variables U and the shock geometry S simultaneously in an implicit manner. Using (8), the FIST time discretization takes the form

$$\Delta U^n - c_1 h \Delta(R_1(U^n, S^n)) = c_2 \Delta U^{n-1} + c_3 h R_1(U^n, S^n); \quad 0 < \xi \leq 1, 1 < \xi < k, \quad (9)$$

$$\Delta U_R^n = \Delta(\mathcal{R}(U_L^n, S^n)); \quad \xi = 1, \quad (10)$$

$$\Delta U^n - c_1 h \Delta(R_2(U^n, S^n)) = c_2 \Delta U^n + c_3 h R_2(U^n, S^n); \quad \xi = k, \quad (11)$$

$$\Delta S^n - c_1 h \Delta(R_3(U^n, S^n)) = c_2 \Delta S^{n-1} + c_3 h R_3(U^n, S^n). \quad (12)$$

Here (9) represents interior equations (3), (10) represents shock relations (6), (11) represents the two outflow compatibility conditions of Eq. (5b), and (12) represents (7). When ΔR_i ($i = 1, 2, 3$) and $\Delta \mathcal{R}$ are linearized, the resulting equations remain fully coupled. More precisely, the linearizations involve both U and S ; e.g.,

$$\Delta(R_i(U^n, S^n)) \approx [\partial R_i / \partial U]^n \Delta U^n + [\partial R_i / \partial S]^n \Delta S^n,$$

where $[\partial R_i/\partial U]^n$ and $[\partial R_i/\partial S]^n$ represent the (unique) linear differential operators corresponding to the "derivatives" of R_i with respect to U and S , respectively, taken at (U^n, S^n) . The evaluation of these linearizations will be discussed later in this section.

The problem is discretized spatially using equally spaced points $j = 1, \dots, j_s$ to the left of the shock and $j = j_s + 1, \dots, j_{\max}$ to the right of the shock (see Fig. 1) and replacing spatial derivatives by centered differences at interior points and appropriate one-sided differences at $\xi = 1$ and $\xi = K$. For convenience, the unknowns U at $\xi = 0$ are eliminated by substituting (4) into the discretized equations. The resulting discrete matrix problem for ΔU^n ($j = 2, \dots, j_{\max}$), ΔS^n admits essentially a block tridiagonal solution when the equations and unknowns are suitably ordered. In particular, the linearized system is written with the ordering,

$$\left(I - c_1 h \left[\frac{\partial R_1}{\partial U} \right] \right) \Delta U_j^n - c_1 h \left[\frac{\partial R_1}{\partial S} \right] \Delta S^n = c_2 \Delta U_{j-1}^n + c_3 h R_1^n \quad (j = 2, \dots, j_s),$$

$$\Delta U_{j_s+1}^n - [\partial \mathcal{R}/\partial U_L] \Delta U_{j_s}^n - [\partial \mathcal{R}/\partial S] \Delta S^n = 0,$$

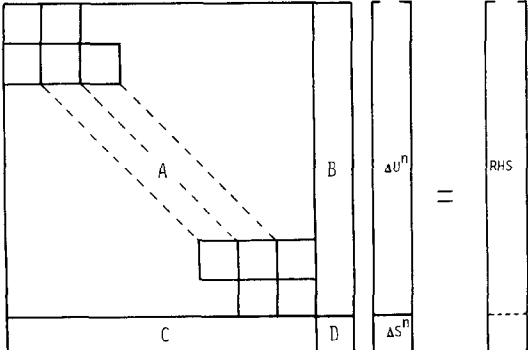
$$\left(I - c_1 h \left[\frac{\partial R_1}{\partial U} \right] \right) \Delta U_j^n - c_1 h \left[\frac{\partial R_1}{\partial S} \right] \Delta S^n = c_2 \Delta U_{j-1}^n + c_3 h R_1^n \quad (j = j_s + 1, \dots, j_{\max} - 1),$$

$$\Delta U_{1, j_{\max}}^n + (A(x_{\max})/(K-1)) \rho_e \Delta S^n = 0,$$

$$\left(I - c_1 h \left[\frac{\partial R_2}{\partial U} \right] \right) \Delta U_{i, j_{\max}}^n - c_1 h \left[\frac{\partial R_2}{\partial S} \right] \Delta S^n = c_2 \Delta U_{i, j_{\max}-1}^n + c_3 h R_2^n \quad (i = 2, 3),$$

$$-c_1 h \left[\frac{\partial R_3}{\partial U} \right] \Delta U^n + \left(I - c_1 h \left[\frac{\partial R_3}{\partial S} \right] \right) \Delta S^n = c_2 \Delta S^{n-1} + c_3 h R_3^n.$$

Writing the system in this way yields an algebraic system of the form



$$(13)$$

where \mathbf{A} is a block tridiagonal matrix with $(j_{\max} - 1)$ rows of blocks of size 3×3 , \mathbf{B} is $3(j_{\max} - 1) \times 2$, \mathbf{C} is $2 \times 3(j_{\max} - 1)$, and \mathbf{D} is 2×2 . This system is solved using a block inversion procedure as found in [9] (see Appendix C for details). After the solution of (13) is obtained, $U_{j_s+1}^{n+1}$ is redefined using (6) to ensure that the Rankine-Hugoniot conditions are satisfied.

Explicit Shock Tracking (EST)

For comparison purposes, we consider an algorithm EST in which the shock quantities S are *not* treated implicitly. Preliminary experimentation with several ways of explicitly treating the unknowns S indicated that the following method showed the best convergence behavior: First, the conservation variables U are advanced implicitly using (9)–(11) linearized with S fixed at S^n , subject to boundary conditions (4) and (5a) with $s = s^n$. The discrete algebraic system for ΔU^n ($j = 2, \dots, j_{\max}$) is $\mathbf{A} \Delta U^n = \text{RHS}$, where the matrix \mathbf{A} is the same as in (13). Next, S is advanced explicitly using

$$s_i^{n+1} = s_i^n + hr_3(U^{n+1}, S^n), \quad s^{n+1} = s^n + hs_i^{n+1}.$$

The final step, as in FIST, is to redefine $U_{j_s+1}^{n+1}$ using (6) with $U_{j_s}^{n+1}, S^{n+1}$.

Alternating Unknown Implicit (AUI)

We also consider a compromise approach in which some of the implicit character of the shock advancement is maintained. In essence the method alternates the unknowns which are treated implicitly (AUI). First, the variables U are advanced implicitly keeping the shock fixed as in EST. Next, the shock variables S are advanced implicitly keeping U fixed at U^{n+1} using

$$(I - c_1 h[\partial R_3/\partial S]) \Delta S^n = c_2 \Delta S^{n-1} + h[c_1 R_3(U^{n+1}, S^n) + (c_3 - c_1) R_3(U^n, S^n)].$$

Finally, as in FIST and EST, $U_{j_s+1}^{n+1}$ is redefined using (6). As will be discussed in Section 4, this method allows a larger time step than EST with no significant increase in computational time. For this reason AUI may be a valuable tool for multidimensional problems where operator splitting limits the time step.

Numerical Linearization

Implementation of all the above methods requires evaluations of various Jacobian matrices. Indeed, suppose we consider the differential operator $\partial G/\partial \xi$, where $G = G(V)$ and $V = V(\xi)$ are vector-valued functions. Then the linearization of $\partial G/\partial \xi$ with respect to V is given by

$$\left[\frac{\partial}{\partial V} \left(\frac{\partial G}{\partial \xi} \right) \right]_j = \left(\frac{\partial}{\partial \xi} \left[\frac{\partial G}{\partial V} \right] \right)_j \approx \left(\left[\frac{\partial G}{\partial V} \right]_{j+1} - \left[\frac{\partial G}{\partial V} \right]_{j-1} \right) / (2 \Delta \xi),$$

where $[\partial G/\partial V]$ is the Jacobian matrix of G with respect to V . In principle, for a perfect gas, analytic expressions can be obtained for the required Jacobian matrices.

An alternative approach is to directly evaluate the Jacobians numerically (to order of the square root of machine error) by replacing the derivatives with respect to the components of V by appropriate first-order forward differences. This direct numerical approach is used in the present study. It is simpler to program (especially for FIST) and appears to cause little or no difference in quality of results or execution time. Note that, using the direct numerical approach, the formation of the matrix for FIST requires essentially six evaluations of R_i ($i = 1, 2, 3$) and \mathcal{R} (since U and S contain a total of 5 components). This is comparable to four evaluations for EST and AUI and 2 evaluations for an explicit predictor–corrector method.

4. NUMERICAL RESULTS

We now present our computational results for the duct flow problem, assessing first the accuracy of the steady-state finite difference solution, and then the computational efficiencies of the various methods (FIST, EST, and AUI). For the purposes of further comparison, we also compare with the explicit predictor–corrector method of Brailovskaya; see Appendix D. (For the present problem, this method converges faster than the second-order accurate MacCormack scheme, and also enjoys the advantage that it reduces to the same steady-state difference equations as do the other methods tested here.) In the numerical experiments, the duct shape was taken to be $A(x) = 1.398 + 0.347(\tanh(0.8x - 4.))$, with $x_{\max} = 10$. In all cases we take $K = 2$, $\gamma = 1.4$, $\rho_0 = 0.502$, $u_0 = 1.299$, $e_0 = 1.897$, and $\rho_e = 0.776$, and we use Euler implicit time differencing (i.e., $c_1 = c_3 = 1$, $c_2 = 0$). We use two different initial guesses, hereafter referred to as the “good guess” and “bad guess.” The good guess is the exact steady state solution for a slightly perturbed duct shape, cf. [6]. The bad guess is an exact solution for flow in the given duct $A(x)$ but with a different downstream density ρ_e specified. In our experiments, the outflow condition $\rho_e = 0.776$ was imposed impulsively at $t = 0$. Figures 2a and b illustrate the quality of the pressure profiles for the two guesses relative to the exact steady-state solution. The steady-state solution of the difference equations (obtained with any of the methods) is shown in Figs. 3a and b for $j_{\max} = 18$ and 34, respectively. In the latter case the numerical solution is virtually indistinguishable from the exact solution. We wish to emphasize that, in these results and all those that follow, *no numerical dissipation* was used.

In comparing the efficiencies of the various methods, we shall refer to runs made with time steps corresponding to various multiples of the CFL (Courant, Friedrichs, Levy) number, defined to be $\omega \Delta\tau/\Delta\xi$, where ω is the maximum over all j of the spectral radius of $[\partial F/\partial U]_j$. We first determine the approximate maximum value of CFL at which each of the methods will run with $j_{\max} = 34$ and when started with the good or bad guess (Table I). We note that, as expected, FIST approaches Newton’s method in the limit of large time steps. Indeed, with $\text{CFL} = 10^6$, FIST converged in 5 iterations to steady-state tolerances within machine error (10^{-13}) when started with the good guess.

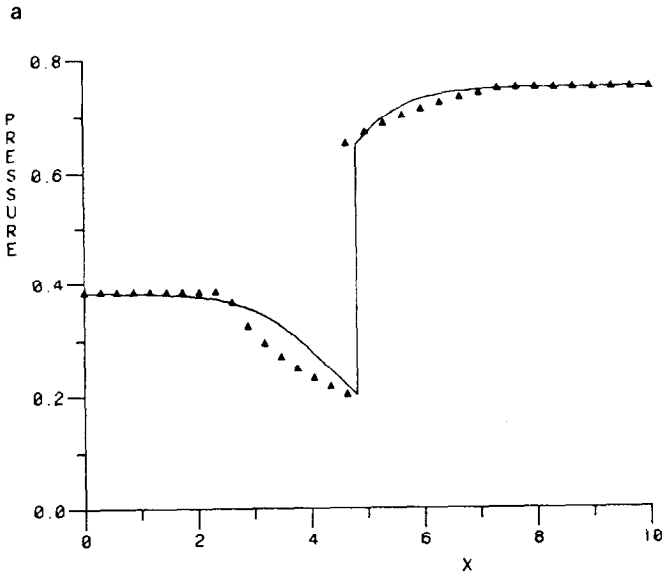


FIG. 2a. Good guess (▲) versus exact steady state solution (-).

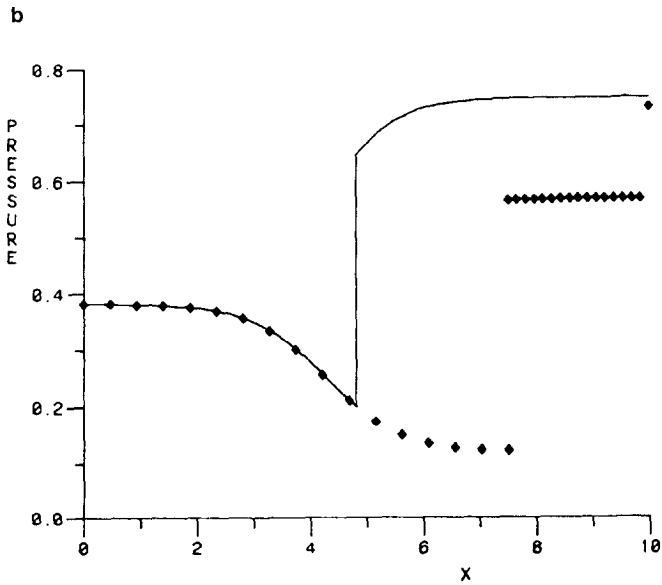


FIG. 2b. Bad guess (◆) versus exact steady state solution (-).

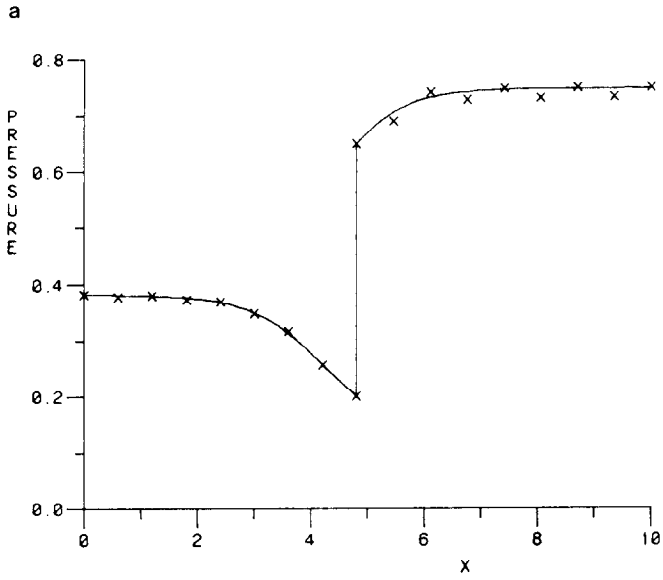


FIG. 3a. Steady state difference solution (x) with $j_{\max} = 18$ versus exact solution (-).

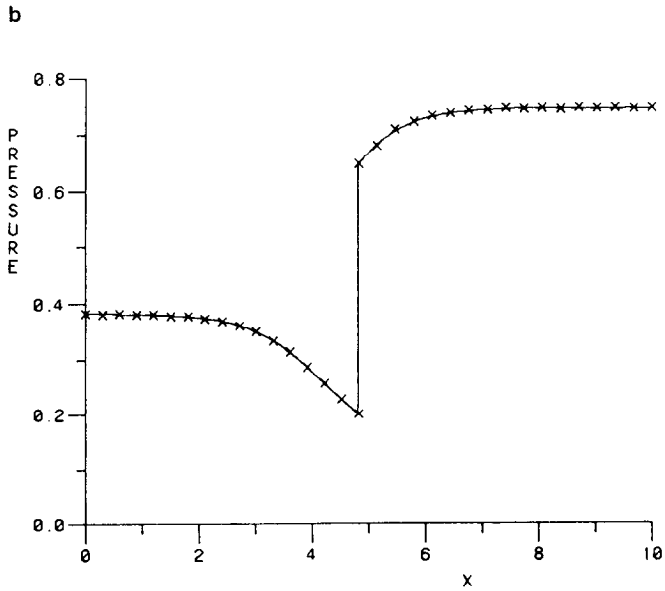


FIG. 3b. Steady state difference solution (x) with $j_{\max} = 34$ versus exact solution (-).

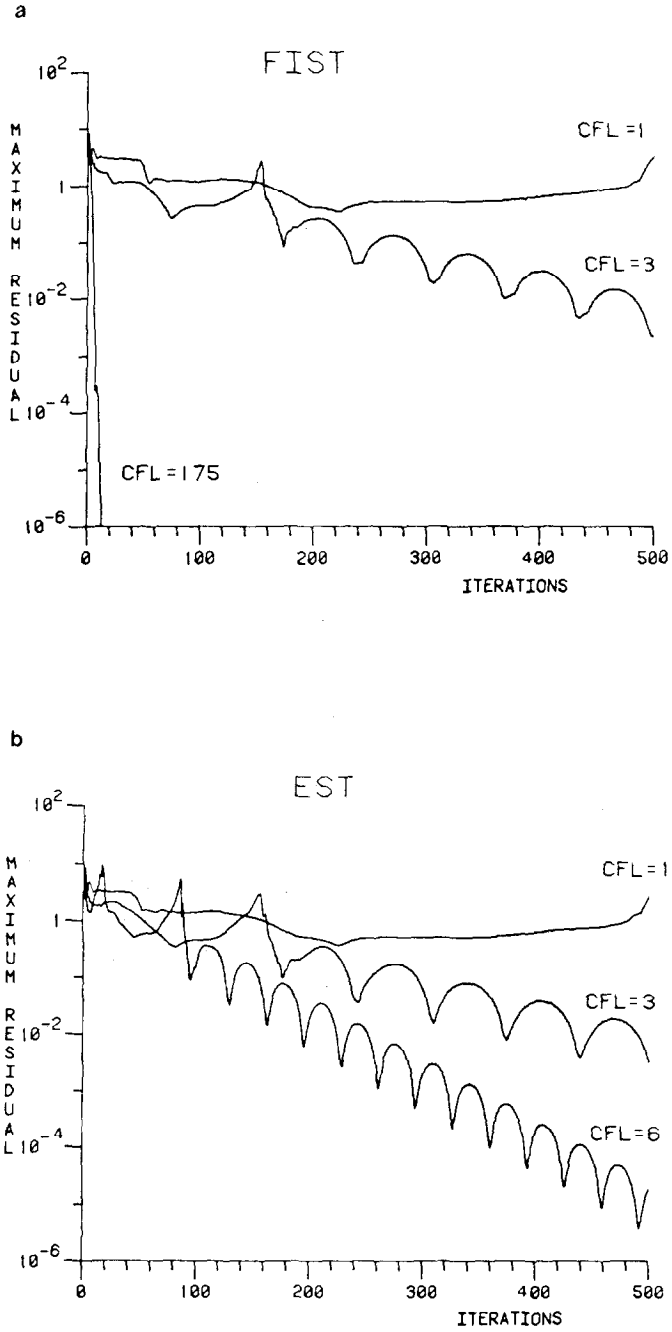


FIGURE 4

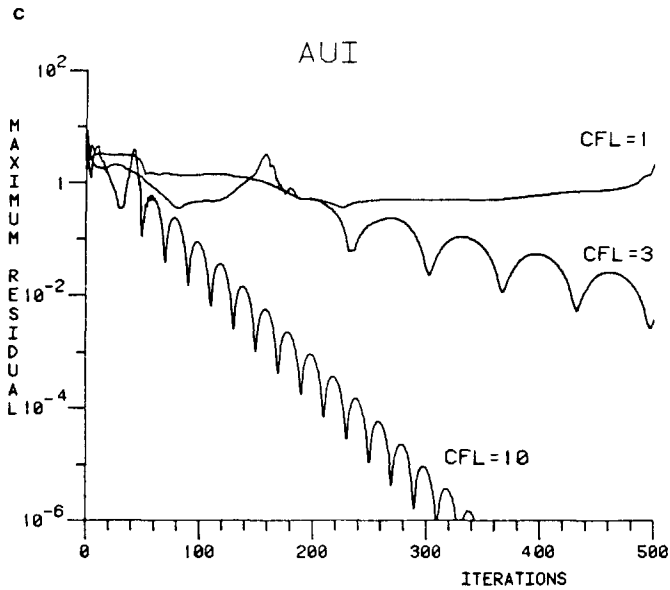


FIG. 4 (continued)

We next examine convergence behavior for the various methods. We plot maximum residual (value obtained by substituting the current difference solution into the steady-state difference equations) versus either iterations or computer time. Computer time will be based on units where one unit is the time necessary for one step of the Brailovskaya method (see Table I). We note that in implementing FIST, EST, and AUI, the inversion of matrix A was actually obtained using a banded solver rather than a block tridiagonal solver. This was done because the block tridiagonal decomposition could become ill conditioned at large values of CFL.

We first look at runs made with FIST, EST, and AUI at various values of CFL (Figs. 4a-c). In all cases, the bad guess was used and $j_{\max} = 34$. As usually assumed, each method converges in fewer iterations as the CFL factor becomes larger. (It is

TABLE I

Method	Max CFL good guess	Max CFL bad guess	Time units per iteration
Brailovskaya	1	1	1
EST	9	6	3.4
AUI	10	10	3.5
FIST	10^{10}	175	4.8

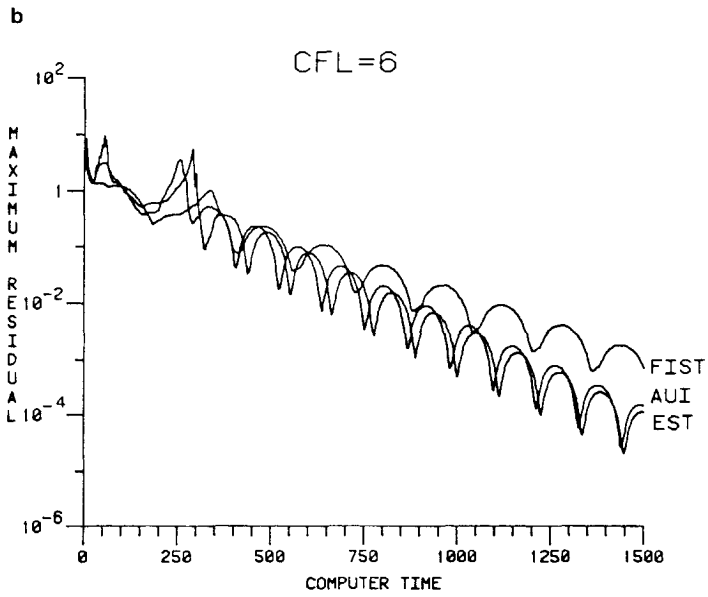
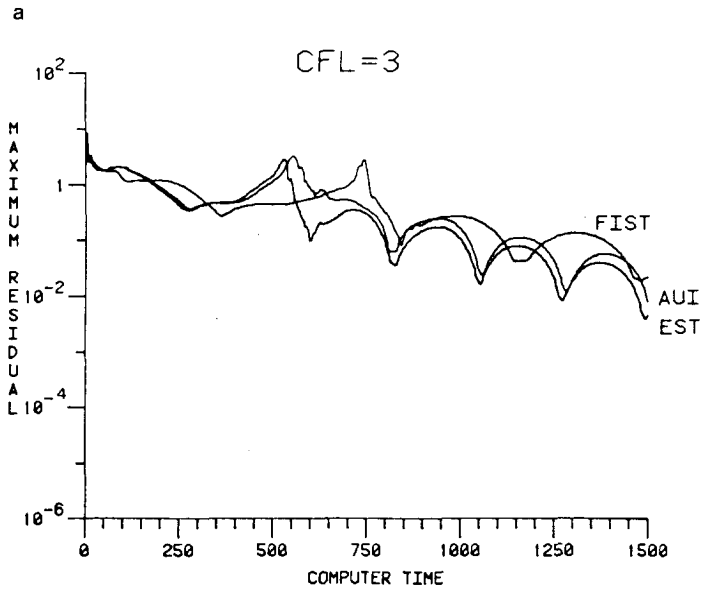


FIGURE 5

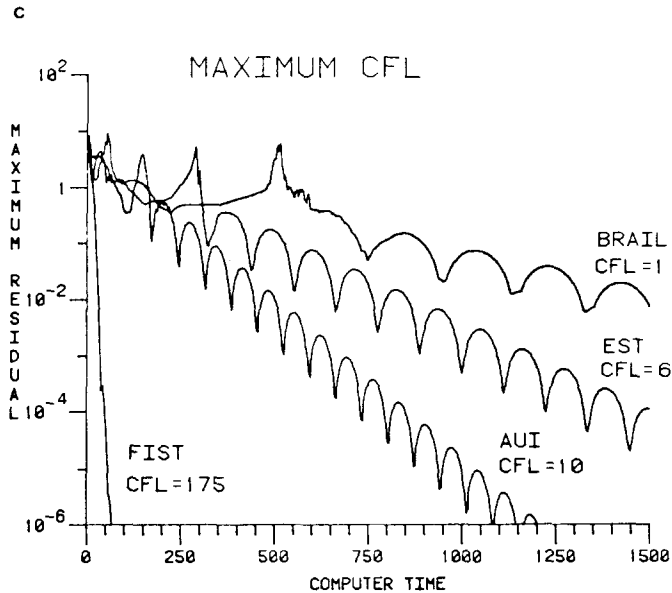


FIG. 5 (continued)

interesting to note that starting with the good guess, it is possible to find CFL values for which EST and AUI oscillate between two states instead of converging.) When compared with respect to computer time at fixed CFL = 3 and 6 (Figs. 5a and b), we see that there is very little difference between EST and AUI, and that the extra work per iteration needed in FIST does not pay off in faster convergence. When compared at their maximum allowable CFL values (Fig. 5c), however, the FIST method is clearly superior.

5. CONCLUDING REMARKS

As demonstrated by the numerical results, for one-dimensional problems the FIST approach produces significant increases in computational efficiency when compared with purely explicit methods and with implicit methods using explicit shock tracking. In some sense, this comparison is unfair since for very large time steps FIST approaches Newton's method for solving the difference analog of the steady state equations, and thus exhibits quadratic convergence behavior. In fact, the FIST approach combines the advantages in computational efficiency of Newton's method with the robustness of time asymptotic methods.

The implications of the present study for multidimensional problems are difficult to

assess. This is especially true if operator splitting or factorization is used. It is not clear how the various methods will compare with respect to computer time needed per iteration, or how large the maximum allowable CFL values will be. Two competing factors affect the computational time per iteration. Assuming a single shock, the fully coupled implicit shock treatment will occur in only one of the directional sweeps. The number of variables needed to specify the shock geometry and movement will increase, however. The maximum allowable CFL values for each method are problem dependent and will certainly be limited by splitting error. Since FIST will no longer reduce to Newton’s method in this framework, the suitability of the various methods depends on the relation between the CFL restriction due to splitting and the CFL restriction due to explicit shock treatment. It is impossible to discern a priori which method will be best.

In closing we note that a split version of FIST is being developed for the supersonic blunt body problem. The results of this work will appear in a forthcoming paper.

APPENDIX A: CHARACTERISTIC ANALYSIS OF THE BOUNDARIES

The background on characteristic theory and characteristic compatibility conditions may be found in [10]. For their application to the treatment of boundaries in fluid dynamics, see [11]. We give here only an outline of the general approach and apply it to system (3).

Since system (3) is hyperbolic, it is equivalent to three characteristic compatibility conditions. These conditions take the form of ordinary differential equations which hold along characteristic curves in (τ, ξ) space. At a boundary of the computational domain, certain of these curves are “admissible” since they reach the boundary from inside the computational domain (when moving along them in the direction of increasing τ). The compatibility conditions associated with these admissible characteristics may be applied as computational boundary conditions. Other characteristic curves are “inadmissible” since they reach the boundary from outside the domain. The compatibility conditions corresponding to these curves must be replaced by specified boundary values.

Specifically, (3) is equivalent to the quasilinear system.

$$\frac{J}{A} L(U) \equiv \frac{J}{A} \left(\frac{\partial U}{\partial \tau} - R_1 \right) = \frac{\partial \mathcal{U}}{\partial \tau} + \mathbb{B} \frac{\partial \mathcal{U}}{\partial \xi} + \frac{1}{A} \left(\frac{dA}{dx} \mathcal{F} - \mathcal{K} \right) \equiv \mathcal{L}(\mathcal{U}) = 0, \tag{A1}$$

where $\mathbb{B} = \xi_t I + \xi_x [\partial \mathcal{F} / \partial \mathcal{U}]$, and $[\partial \mathcal{F} / \partial \mathcal{U}]$ is the Jacobian matrix of \mathcal{F} with respect to \mathcal{U} . The characteristic matrix associated with (A1) is

$$\mathbb{C}(\lambda_0, \lambda_1) \equiv \lambda_0 I + \lambda_1 \mathbb{B} \tag{A2}$$

$$= \begin{pmatrix} A_0 & A_1 & 0 \\ \frac{1}{2}(\gamma - 3)A_1 u^2 & A_0 - A_1(\gamma - 3)u & A_1(\gamma - 1) \\ -A_1 u \left(\frac{a^2}{\gamma - 1} - \frac{\gamma - 2}{2} u^2 \right) & A_1 \left[\frac{a^2}{\gamma - 1} - (\gamma - \frac{3}{2}) u^2 \right] & A_0 + \gamma u A_1 \end{pmatrix},$$

where $A_0 = \lambda_0 + \lambda_1 \xi_t$, $A_1 = \lambda_1 \xi_x$, and a is the speed of sound. A characteristic curve $\Phi(\xi, \tau) = \text{const}$ satisfies the characteristic condition

$$\det \mathbb{C} = \sigma(\sigma^2 - a^2 A_1^2) = 0, \tag{A3}$$

where $\sigma = A_0 + u A_1$, $\lambda_0 = \Phi_\tau$, and $\lambda_1 = \Phi_\xi$. The slopes of the characteristic curves $\mathcal{C}_0, \mathcal{C}_\pm$ associated with the three distinct characteristic conditions $\sigma_0 = 0, \sigma_\pm = \pm a A_1$ are given, respectively, by

$$\mathcal{C}_0: d\xi/d\tau = q, \quad \mathcal{C}_\pm: d\xi/d\tau = q \mp a \xi_x, \tag{A4}$$

where $q = \xi_t + u \xi_x$. The \mathcal{C}_0 curve is a particle path and the \mathcal{C}_\pm curves represent Mach (or sound) waves. Corresponding to the three characteristic conditions are three independent left null vectors (defined by $\mathbf{l} \cdot \mathbb{C} = 0$) given by

$$\mathbf{l}_0 = \left(\frac{u^2}{2} - \frac{a^2}{\gamma - 1}, -u, 1 \right), \quad \mathbf{l}_\pm = \left(\frac{\pm u^2}{2} + \frac{au}{\gamma - 1}, \frac{-a}{\gamma - 1} \mp u, \pm 1 \right). \tag{A5}$$

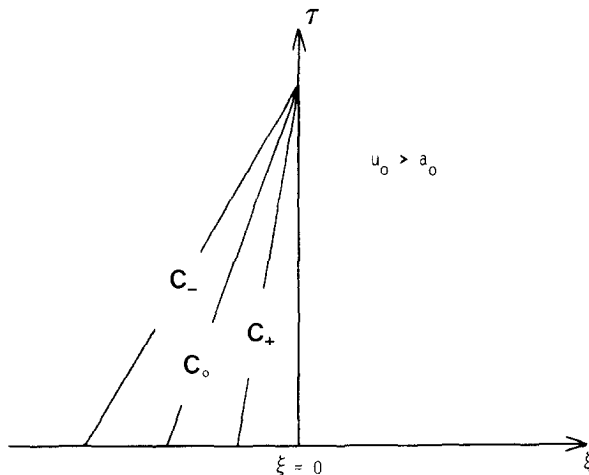


FIG. A1. Characteristic slopes at $\xi = 0$ for supersonic inflow.

The three characteristic compatibility conditions holding along the characteristic curves are obtained by left multiplying (A1) by I_0 and I_{\pm} in the form

$$I \cdot L(U) = 0 \quad \text{or} \quad I \cdot \mathcal{L}(\mathcal{U}) = 0. \tag{A6}$$

Inflow and Outflow Boundaries

At the inflow boundary $\xi = 0$, we assume the flow to be supersonic ($u > a$). Since $\xi_t = 0$ and $\xi_x > 0$ at $\xi = 0$, it follows from (A4) that the characteristic slopes are as depicted in Fig. A1. Hence, none of the characteristics are admissible and accordingly all the flow variables must be specified at $\xi = 0$.

At the outflow boundary $\xi = K$, we assume subsonic flow ($0 < u < a$). In this case, the characteristic slopes are depicted in Fig. A2. Hence, at $\xi = K$, the compatibility conditions associated with the admissible characteristics \mathcal{C}_0 and \mathcal{C}_- should be satisfied and one flow variable must be specified. Although several possibilities exist, we specify the density ρ_e at outflow. This leads to (5a) for the first component of U on $\xi = K$. The derivative of (5a) with respect to τ and compatibility conditions (A6) for \mathcal{C}_0 and \mathcal{C}_- give the following system on $\xi = K$:

$$\begin{aligned} \mathbf{T}_0 \left(\frac{\partial U}{\partial \tau} \right)_{\xi=K} &= -\mathbf{T}_1 \left(\frac{\partial F}{\partial \xi} - \frac{1}{J} \mathcal{H} \right)_{\xi=K} \\ &+ \frac{A(x_{\max})}{K-1} \left[\frac{d\rho_e}{dt} (x_{\max} - s) - \rho_e s_t \right] \begin{pmatrix} 1 \\ 0 \\ 0 \end{pmatrix}, \end{aligned}$$

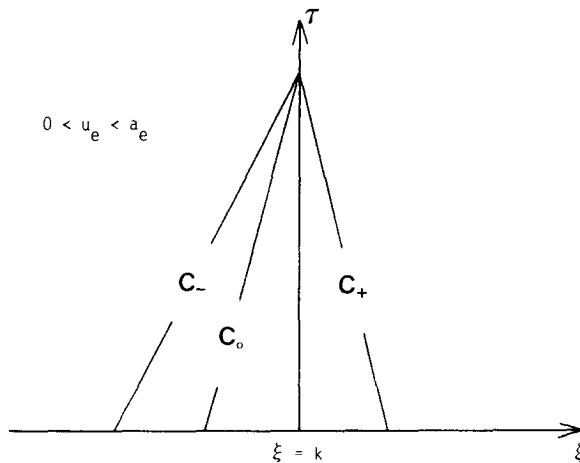


FIG. A2. Characteristic slopes at $\xi = K$ for subsonic outflow.

where

$$\mathbf{T}_0 = \begin{pmatrix} 1 & 0 & 0 \\ \frac{1}{2}u^2 - (a^2/(\gamma - 1)) & -u & 1 \\ ((a/(\gamma - 1)) - \frac{1}{2}u)u & u - (a/(\gamma - 1)) & -1 \end{pmatrix}_{\xi=K}, \quad \mathbf{T}_1 = \mathbf{T}_0 - \begin{pmatrix} 1 & 0 & 0 \\ 0 & 0 & 0 \\ 0 & 0 & 0 \end{pmatrix}$$

The above can be solved for $(\partial U_2/\partial \tau)_{\xi=K}$ and $(\partial U_3/\partial \tau)_{\xi=K}$. The result is given in (5b).

Shock Wave Boundaries

The shock wave $\xi = 1$ is an internal computational boundary. We first analyze each side separately and then combine the results appropriately. We assume that the flow crosses the shock from left (L) to right (R) which implies that the left side of $\xi = 1$ is the low pressure side. In addition we have that $w_L = u_L - s_t > a_L$ and $0 < w_R = u_R - s_t < a_R$ (see, e.g., [12]). Since on both sides of $\xi = 1$, $\xi_t = -\xi_x s_t$ and $\xi_x > 0$, it follows from (A4) that the characteristic slopes on each side of $\xi = 1$ are as depicted in Fig. A3.

For the left side of $\xi = 1$, all the compatibility conditions should be satisfied, cf., Fig. A3a. This is equivalent to satisfying the full system (3) on the left side of $\xi = 1$ (with the ξ -derivatives interpreted using quantities only to the left side of $\xi = 1$).

For the right side of $\xi = 1$, only the compatibility condition corresponding to \mathcal{C}_+ should be satisfied; cf., Fig. A3b. The form of this compatibility condition used in this study is obtained from the second expression in (A6). Noting that $(\lambda_0/\lambda_1)_R \mathbf{1}_+ = -\mathbf{1}_+ \cdot \mathbb{B}$ and that $(\lambda_0/\lambda_1)_R = -(\xi_x)_R(w_R - a_R)$, we obtain

$$\mathbf{1}_+ \cdot \left(\frac{\partial \mathcal{U}}{\partial \tau} \right)_R = -(\xi_x)_R(w_R - a_R) \mathbf{1}_+ \cdot \left(\frac{\partial \mathcal{U}}{\partial \xi} \right)_R - \frac{1}{A} \left[\mathbf{1}_+ \cdot \left(\frac{dA}{dx} \mathcal{F} - \mathcal{H} \right) \right]_R. \tag{A7}$$

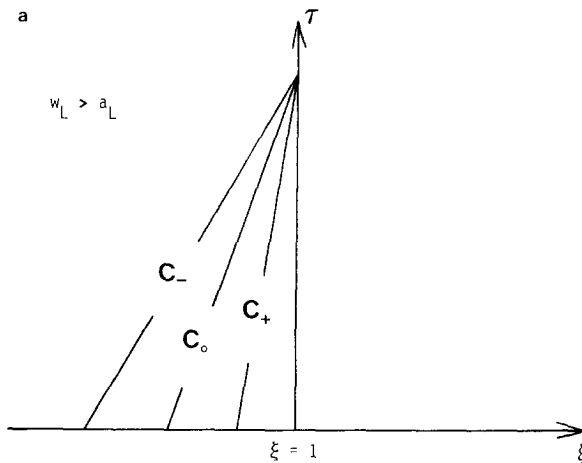


FIG. A3a. Characteristic slopes on the left (low pressure) side of $\xi = 1$.

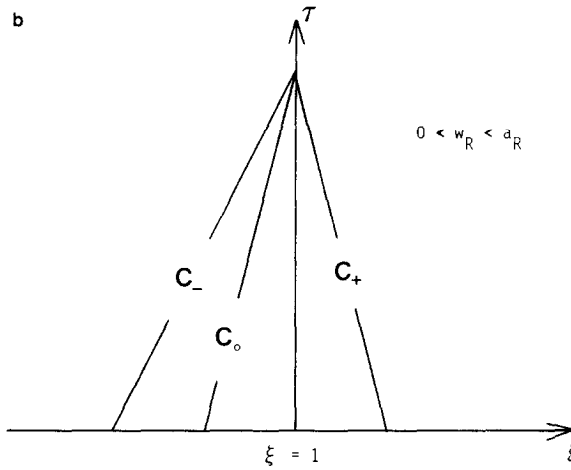


FIG. A3b. Characteristic slopes on the right (high pressure) side of $\xi = 1$.

Here \mathbf{I}_+ is evaluated at the right side of the shock. The left side of (A7) can be written in terms of $Q = (p, u, \rho)^t$ as

$$\mathbf{I}_+ \cdot (\partial \mathcal{Z} / \partial \tau)_R = \mathbf{I}_+ \cdot [\partial \mathcal{Z} / \partial Q]_R^{-1} (\partial Q_R / \partial \tau) = (1/(\gamma - 1)) [(\partial p / \partial \tau) - a \rho (\partial u / \partial \tau)]_R, \tag{A8}$$

where $[\partial \mathcal{Z} / \partial Q]$ is the Jacobian matrix of \mathcal{Z} with respect to Q which, for a perfect gas, can be obtained by direct calculation. In (A8), the derivatives of p_R and u_R can be eliminated using the Rankine-Hugoniot relations, (B1) of Appendix B, differentiated with respect to τ . The result is

$$(\gamma - 1) \mathbf{I}_+ \cdot (\partial \mathcal{Z} / \partial \tau)_R = -c_0 (\partial s_i / \partial \tau) + b_1 (\partial p_L / \partial \tau) + b_2 (\partial \rho_L / \partial \tau) + b_3 (\partial u_L / \partial \tau), \tag{A9}$$

where

$$\begin{aligned} c_0 &= [(\rho_R - \rho_L) / (w_R - a_R)] [(\gamma - 1) w_R (w_L - w_R) - a_R (w_R + a_R)], \\ b_1 &= [\gamma (w_L - w_R) / (w_R - a_R)] + 1, \\ b_2 &= [1 / (w_R - a_R)] \{ a_R^2 w_R - a_L^2 w_L - (w_L - w_R) [(\gamma - 1) w_L w_R + a_R (w_L - a_R)] \}, \\ b_3 &= c_0 - a_R \rho_R. \end{aligned}$$

An expression for the τ derivatives of p_L , u_L , and ρ_L required in (A9) can be obtained from the differential equations on the left side of $\xi = 1$ in the form

$$\frac{\partial Q_L}{\partial \tau} = - \left[\frac{\partial \mathcal{R}}{\partial Q} \right]_L^{-1} \left\{ \mathbb{B} \frac{\partial \mathcal{R}}{\partial \xi} + \frac{1}{A} \left[\frac{dA}{dx} \mathcal{F} - \mathcal{H} \right] \right\}_L. \quad (\text{A10})$$

Combining A7–A10 gives, after some manipulation, the final result

$$\partial s_i / \partial \tau = \alpha_1 \cdot (\partial \mathcal{R} / \partial \xi)_R - \alpha_2 \cdot (\partial \mathcal{R} / \partial \xi)_L + \alpha_3 ((1/A)(dA/dx))_{\xi=1},$$

where

$$\alpha_1 = (1/c_0)(\gamma - 1)(\xi_x)_R (w_R - a_R) \left[\frac{1}{2} u_R^2 + (a_R/(\gamma - 2)) u_R, -u_R - (a_R/(\gamma - 1)), 1 \right],$$

$$\alpha_2 = \frac{(\xi_x)_L}{c_0} \left[u_L b_1 \left(\frac{\gamma - 1}{2} u_L w_L - a_L^2 \right) + \frac{u_L}{\rho_L} b_3 \left(\frac{\gamma - 1}{2} u_L - w_L \right) \right.$$

$$\left. + b_2 (w_L - u_L), \right.$$

$$b_1 (a_L^2 - (\gamma - 1) u_L w_L) + \frac{b_3}{\rho_L} (w_L - (\gamma - 1) u_L) + b_2,$$

$$\left. (\gamma - 1) \left(w_L b_1 + \frac{b_3}{\rho_L} \right) \right],$$

$$\alpha_3 = (1/c_0) [\gamma p_R u_R - u_L (\gamma p_L b_1 + \rho_L b_2)].$$

APPENDIX B: RANKINE–HUGONIOT SHOCK RELATIONS

We give here the jump conditions across the shock in terms of the U variables and s, s_t . For a perfect gas, we have (cf. [12])

$$Q_R \equiv \begin{pmatrix} p_R \\ u_R \\ \rho_R \end{pmatrix} = \begin{pmatrix} p_L (\gamma \beta M^2 + 1) \\ u_L - (u_L - s_t) \beta \\ \rho_L / (1 - \beta) \end{pmatrix} \equiv \mathbf{f}(Q_L, s_t), \quad (\text{B1})$$

where

$$M^2 = (u_L - s_t)^2 \rho_L / (\gamma p_L) \quad \text{and} \quad \beta = 2(M^2 - 1) / [(\gamma + 1) M^2].$$

Since on the left side (subscript L) of the shock $\xi_x = 1/s$,

$$Q_L \equiv \begin{pmatrix} p_L \\ u_L \\ \rho_L \end{pmatrix} = \begin{pmatrix} \frac{(\gamma - 1)}{sA(s)} \left(U_3 - \frac{U_2^2}{2U_1} \right)_L \\ (U_2/U_1)_L \\ (U_1)_L / [sA(s)] \end{pmatrix} \equiv \mathbf{g}(U_L, s). \quad (\text{B2})$$

On the right side (subscript R) of the shock $\xi_x = (K - 1)/(x_{\max} - s)$ which implies

$$U_R = \frac{(x_{\max} - s) A(s)}{K - 1} \begin{pmatrix} \rho_R \\ \rho_R u_R \\ p_R/(\gamma - 1) + \rho_R u_R^2/2 \end{pmatrix} \equiv \mathbf{h}(Q_R, s). \tag{B3}$$

We therefore have

$$U_R = \mathcal{R}(U_L, s, s_t) = \mathbf{h}(\mathbf{f}(\mathbf{g}(U_L, s), s_t), s).$$

APPENDIX C: INVERSION ALGORITHM FOR EQ. (13)

Here we give a 2×2 block matrix inversion algorithm for the system,

$$\begin{bmatrix} \boxed{A} & \boxed{B} \\ \boxed{C} & \boxed{D} \end{bmatrix} \begin{bmatrix} y \\ z \end{bmatrix} = \begin{bmatrix} f_1 \\ f_2 \end{bmatrix}$$

where **D** is very small (in the present context 2×2) and **A** admits a convenient *L-U* factorization (in this case **A** is block tridiagonal).

Following [9] observe that

$$\mathbf{A}y + \mathbf{B}z = f_1 \tag{C1}$$

and

$$\mathbf{C}y + \mathbf{D}z = f_2. \tag{C2}$$

Then from (C1),

$$y = \mathbf{A}^{-1}f_1 - (\mathbf{A}^{-1}\mathbf{B})z. \tag{C3}$$

Substitution of (C3) into (C2) yields

$$\mathbf{C}(\mathbf{A}^{-1}f_1) - \mathbf{C}(\mathbf{A}^{-1}\mathbf{B})z + \mathbf{D}z = f_2$$

or

$$z = (\mathbf{D} - \mathbf{C}\mathbf{A}^{-1}\mathbf{B})^{-1}(f_2 - \mathbf{C}\mathbf{A}^{-1}f_1). \tag{C4}$$

Substitution of (C4) into (C3) yields

$$y = \mathbf{A}^{-1}f_1 - \mathbf{A}^{-1}\mathbf{B}(\mathbf{D} - \mathbf{C}\mathbf{A}^{-1}\mathbf{B})^{-1}(f_2 - \mathbf{C}\mathbf{A}^{-1}f_1). \quad (\text{C5})$$

Note that in the evaluation of (C4) and (C5), $\mathbf{A}^{-1}f_1$ and $\mathbf{A}^{-1}\mathbf{B}$ are obtained simultaneously; indeed, the evaluation of $\mathbf{A}^{-1}f_1$ is a standard inversion technique and the computation of $\mathbf{A}^{-1}\mathbf{B}$ requires only one extra backsolve for each column of \mathbf{B} . Theoretical work estimates indicate that (for the case when \mathbf{D} is 2×2) the evaluation of $\mathbf{A}^{-1}\mathbf{B}$ increases the work by only 60% over that required for $\mathbf{A}^{-1}f_1$. By design, $\mathbf{D} - \mathbf{C}\mathbf{A}^{-1}\mathbf{B}$ is a small matrix and thus easily inverted.

APPENDIX D: THE BRAILOVSKAYA SCHEME

The Brailovskaya scheme [13] (also known as the Matsuno scheme) for the system $U_\tau + F_\xi + H = 0$ is given by the following explicit predictor–corrector sequence:

$$\begin{aligned} (\text{predictor}) \quad U_j^* &= U_j^n - \Delta\tau[(F_{j+1}^n - F_{j-1}^n)/(2\Delta\xi) + H_j^n], \\ (\text{corrector}) \quad U_j^{n+1} &= U_j^n - \Delta\tau[(F_{j+1}^* - F_{j-1}^*)/(2\Delta\xi) + H_j^*], \end{aligned}$$

where F_j^* , H_j^* are evaluated at τ^{n+1} using U_j^* . For the differential equations (5b) and (7), the above scheme is used with appropriate one-sided ξ differences. The formal truncation error of this scheme is $O(\Delta\tau, \Delta\xi^2)$ and a sufficient stability (von Neumann) condition is $\text{CFL} \leq 1$ (cf. Section 4).

REFERENCES

1. R. M. BEAM AND R. F. WARMING, *J. Comput. Phys.* **22** (1976), 87.
2. J. L. STEGER, "Implicit Finite Difference Simulation of Flow About Arbitrary Geometries with Application to Airfoils," AIAA Paper 77-665, presented at Albuquerque, N.M., June 27–29, 1977.
3. T. H. PULLIAM AND D. S. CHAUSSEE, *J. Comput. Phys.* **39** (1981), 347.
4. P. KUTLER, S. R. CHAKRAVARTHY, AND C. P. LOMBARD, "Supersonic Flow Over Ablated Nosetips Using an Unsteady Implicit Numerical Procedure," AIAA Paper 78-213, presented at Huntsville, Ala., Jan. 16–18, 1978.
5. W. R. BRILEY AND H. McDONALD, *J. Comput. Phys.* **34** (1980), 54.
6. G. R. SHUBIN, A. B. STEPHENS, AND H. M. GLAZ, *J. Comput. Phys.* **39** (1981), 364.
7. H. VIVIAND, *Rech. Aerosp.* **1** (1974), 65.
8. R. F. WARMING AND R. M. BEAM, in "Proceedings, SIAM–AMS Symposium on Computational Fluid Dynamics," New York, April 16–17, 1978, 15–129.
9. E. ISAACSON AND H. B. KELLER, "Analysis of Numerical Methods," pp. 58–61, Wiley, New York, 1966.
10. R. COURANT AND D. HILBERT, "Methods of Mathematical Physics," Vol. 2, pp. 599–605, Interscience, New York, 1962.

11. C. P. KENTZER, *in* "Proceedings of Second Internat. Conf. on Numerical Methods in Fluid Dynamics, Univ. of Calif., Berkeley, 1970," Springer-Verlag, New York/Berlin, 1971, 108.
12. L. D. LANDAU AND E. M. LIFSHITZ, "Fluid Mechanics," pp. 317-331, Addison-Wesley, Reading, Mass., 1959.
13. P. ROACHE, "Computational Fluid Dynamics," Hermosa, Albuquerque, N.M., 1972.